Effects of shell correction on α decay properties*

Jing Zhang(张竞)[1] De-Jun E(鄂得俊)[1] Hong-Fei Zhang(张鸿飞)[1,2;1)]

[1] School of Nuclear Science and Technology, Lanzhou University, Lanzhou 730000, China
[2] Joint Department for Nuclear Physics, Lanzhou University and Institute of Modern Physics CAS, Lanzhou 730000, China

Abstract: The shell correction effects on the α decay properties of heavy and superheavy nuclei have been studied in a macroscopic-microscopic manner. The macroscopic part is constructed from the generalized liquid drop model (GLDM), whereas the microscopic part, namely, the shell correction energy, brings about certain effects on the potential barriers and half-lives under a WKB approximation, which is emphasized in this work. The results show that the shell effects play a significant role in the estimation of the α decay half-lives within the actinide region. Predictions of the α decay half-lives are then generated for superheavy nuclei, which will provide useful information for future experiments.

Keywords: shell correction, α decay, generalized liquid drop model

PACS: 21.10.Tg, 23.60.+e, 27.90.+b **DOI:** 10.1088/1674-1137/42/9/094101

1 Introduction

More than 80 years ago, nuclei were first regarded as tiny fluid drops by Gamow[1]. Since the liquid-drop model (LDM) first came into existence, it has shed light on the bulk nuclear properties and many other related phenomena. In 1935, the well-known binding energy formula of Weizsäcker was discovered[2], and shortly thereafter, in 1939, Bohr and Wheeler successfully described the spontaneous fission process with the LDM being extended to deformed nuclei[3]. More importantly, the LDM is firmly based on empirical facts, such as the saturation of the nuclear interaction and the low compressibility of nuclear matter.

In the 1980s, Royer gradually developed a generalized liquid-drop model (GLDM) by introducing the quasi-molecular shapes (QMS)[4] and proximity term[5] into the traditional LDM, which shed more light on diverse nuclear phenomena, for instance, the process of spontaneous fission[6], fusion[7], cluster radioactivity[8], proton emissions[9], α decay[10], and even ternary fission[11, 12].

Nevertheless, for nuclear models such as the LDM and GLDM, the lack of a detailed consideration of the microscopic structure of atomic nuclei prevents a better reproduction of the experimental results from being obtained. In addition, when these models are extrapolated to an unknown region in a nuclear chart, their neglect of the shell and pairing effects undoubtedly reduces their reliability. Unfortunately, it is always tricky to combine the properties of gross nuclear matter with the microscopic effects arising from the shell structures, particularly for cases with a large deformation. For example, in macroscopic-microscopic models such as the finite-range droplet model (FRDM), the shell correction term is usually obtained independently from the LDM part[13].

There are two prevailing methods with regard to a shell correction, both dating back to the 1960s. In 1966, Myers and Swiatecki made the first substantial progress in the estimation of the shell correction energy. They considered the effects of grouping single-particle states in a degenerate Fermi gas, and consequently provided a semi-empirical relationship, namely, the shell correction energy reaches the maximum value when the nucleus is spherical, which is attenuated by the deviation from the sphere[14]. One year later, Strutinsky provided a new perspective on the relationship between single-particle levels and the energy of a liquid drop, which is the fundamental concept of the Strutinsky method, the predominant method for calculating the shell correction energy[15].

In 1984, Royer took the former approach to estimating the shell effects on the fission potential when involving the proximity energy. In binary fission, single-particle states must be strongly diminished around the saddle shapes owing to the significant resultant repulsive Coulomb force and attractive nuclear force between two

Received 26 March 2018, Revised 15 June 2018, Published online 15 August 2018

∗ Supported by National Natural Science Foundation of China (11675066, 11475050), the Fundamental Research Funds for the Central Universities (lzujbky-2017-ot04) and Feitian Scholar Project of Gansu Province

1) E-mail: zhanghongfei@lzu.edu.cn

fragments, which means that the shell correction effects are not too pronounced, as implied by the formula by Myers and Swiatecki, because of the strong proximity energy[16, and references therein]. However, in the case of an α decay, the interaction between fragments is not too intense at the scission point, where an α particle is tangent to a much heavier spherical nucleus. In addition, some recent studies[17, 18] have also confirmed the effects of the neutron shells $N = 82$ and $N = 126$ on the α decay through a detailed investigation of the α preformation probability. Thus, the shell effects are not negligible in studies on the α decay process.

In this work, we primarily investigate the α decay properties of heavy and superheavy nuclei when the shell effects are fully taken into account. The remainder of this paper is organized as follows. In Section 2, the macro-microscopic method based on the GLDM and the shape-dependent shell correction method is introduced. The calculated results and discussions are presented in Section 3. Finally, a summary of the present study is provided in Section 4.

2 Theoretical methods

2.1 Quasi-molecular shapes

Quasi-molecular shapes reasonably describing the axially symmetric nuclear deformation were given by [7]

$$R^2(\theta)=\begin{cases} a^2\sin^2\theta+c_1^2\cos^2\theta, & 0\leqslant\theta<\dfrac{\pi}{2} \\ a^2\sin^2\theta+c_2^2\cos^2\theta, & \dfrac{\pi}{2}\leqslant\theta<\pi \end{cases}, \tag{1}$$

where c_1 and c_2 are the two radial elongations, and a is the neck radius. Assuming a volume conservation, the two parameters $s_1=a/c_1$ and $s_2=a/c_2$ completely define the shape. For a given decay channel, the ratio η between the radii of the fragments allows us to connect s_1 and s_2 as follows:

$$s_2=\frac{s_1^2}{s_1^2+(1-s_1^2)\eta^2} \quad (s_1,s_2\geqslant 0,\eta\leqslant 1).$$

2.2 Potential energy and dynamic barrier

For a deformed nucleus, with the macro-microscopic approach, the total energy consists of two parts: the macroscopic GLDM energy[7] $E_{\rm GLDM}$ and the microscopic energy $E_{\rm mic}$, namely,

$$E=E_{\rm GLDM}+\delta E_{\rm mic}. \tag{2}$$

The first term is expressed as

$$E_{\rm GLDM}=E_{\rm V}+E_{\rm S}+E_{\rm C}+E_{\rm Prox}. \tag{3}$$

Following the GLDM for deformed nuclei prior to separation, the volume energy $E_{\rm V}$, the surface energy $E_{\rm S}$, and the Coulomb energy $E_{\rm C}$ are given respectively by[7]

$$E_{\rm V}=-15.494(1-1.8I^2)A \text{ MeV}, \tag{4}$$

$$E_{\rm S}=17.9439(1-2.6I^2)A^{2/3}(S/4\pi R_0^2) \text{ MeV}, \tag{5}$$

$$E_{\rm C}=0.6e^2(Z^2/R_0)\times 0.5\int(V(\theta)/V_0)(R(\theta)/R_0)^3\sin\theta{\rm d}\theta, \tag{6}$$

where the relative neutron excess $I=1-2Z/A$, and $V(\theta)$ is the electrostatic potential at the surface. In addition, A,Z,R_0, and V_0 are the mass number, atomic number, radius, and surface potential of the spherical parent nucleus, respectively. The radius R_0 is given by[10]

$$R=(1.28A^{1/3}-0.76+0.8A^{-1/3}) \text{ fm}. \tag{7}$$

This formula allows following the experimentally observed increase of the ratio $r=R/A^{1/3}$ based on the mass.

Regarding the neck prior to separation or the gap after it, an additional term, called the proximity energy, must be added to take into account the interaction between close surfaces. This term is essential to describing the one- to two-body transitions smoothly and to obtaining reasonable fusion barrier heights[7].

$$E_{\rm Prox}(r)=2\gamma\int_{h_{\rm min}}^{h_{\rm max}}\Phi[d(r,h)/b]2\pi h{\rm d}h, \tag{8}$$

where h is the distance varying from the neck radius or zero to the height of the neck border, D is the distance between the surfaces, and $b=0.99$ fm is the surface width. In addition, Φ is the proximity function determined by Feldmeier[19]. The surface parameter γ is the geometric mean between the surface elements of the two nuclei or fragments.

Similarly, when a nucleus breaks into two daughter nuclei, these macroscopic energy terms are as follows:

$$E_{\rm V}=-15.494[(1-1.8I_1^2)A_1+(1-1.8I_2^2)A_2] \text{ MeV}, \tag{9}$$

$$E_{\rm S}=17.9439\left[(1-2.6I_1^2)A_1^{2/3}+(1-2.6I_2^2)A_2^{2/3}\right] \text{ MeV}, \tag{10}$$

$$E_{\rm C}=0.6e^2Z_1^2/R_1+0.6e^2Z_2^2/R_2+e^2Z_1Z_2/r, \tag{11}$$

where $A_{\rm i}$, $Z_{\rm i}$, and $I_{\rm i}$ are the mass number, charge number, and relative neutron excess of the i-th nucleus. Eq. (7) is used again for R_i, and r is the distance between the mass centers.

For clarity, the microscopic part herein is simply the shell correction energy

$$\delta E_{\rm mic}=E_{\rm sh}. \tag{12}$$

In addition, the total shell correction energy changes along with the shape evolution of the parent and daughter nuclei:

$$E_{\rm sh}=E_{\rm sh}^{\rm p}+E_{\rm sh}^{\rm d}. \tag{13}$$

First, the shape-dependent shell correction formula put forward by Myers and Swiatecki[14, 20] is adopted:

$$E_{\rm sh}^{\rm p}=E_{\rm sh}^{\rm p,\,sph}(1-2\alpha^2){\rm e}^{-\alpha^2}, \tag{14}$$

where $E_{\rm sh}^{\rm p,\,sph}$ represents the shell correction energy of a spherical parent nucleus; in addition,

$$\alpha^2=\frac{\int(R(\theta)-R_0)^2{\rm d}\Omega}{4\pi a^2}$$

expresses the deviation of the quasi-molecular shape from an undistorted nucleus, where the range $a=0.32r_0$, and the nucleon radius r_0 is 1.2 fm. The simplest linear form is adopted when determining the correction energy during the formation of the daughter nucleus:

$$E_{\rm sh}^{\rm d}(r)=\frac{r-R_0}{R_{\rm d}+R_\alpha-R_0}E_{\rm sh}^{\rm d,\,sph}, \tag{15}$$

where R_0, $R_{\rm d}$, and R_α are the radii of the parent, daughter nucleus, and α particle, respectively, and $E_{\rm sh}^{\rm d,\,sph}$ represents the spherical daughter shell correction. The shell correction energy applied for a spherical nucleus is calculated using the traditional Strutinsky procedure. The WSBETA code with a central potential in axially deformed Woods-Saxon form[21] is used to obtain the single-particle levels of a nucleus. After the α particle is emitted, we assume that the daughter nucleus is nearly spherical, which results in a constant shell correction energy after separation occurs.

The α decay half-life of a nucleus is calculated based on the WKB barrier penetration probability. The decay constant of the α emitter is simply defined as $\lambda=\nu_0 P$. The assault frequency ν_0 has been taken as $10^{20}s^{-1}$. In addition, the barrier penetrability P is calculated using the action integral

$$P=\exp\left[-\frac{2}{\hbar}\int_{R_{\rm in}}^{R_{\rm out}}{\rm d}r\sqrt{2B(r)(E(r)-E({\rm sphere}))}\right], \tag{16}$$

in which E(sphere) represents the energy of a spherical mother nucleus, and $R_{\rm out}$ is simply $e^2Z_dZ_\alpha/Q_\alpha$, where $R_{\rm in}$ is the radius of the parent nucleus. In addition, the approximation $B(r)=\mu$ has been used, where μ is the reduced mass. The half-life is related to the decay constant λ by

$$T_{1/2}=\frac{\ln 2}{\lambda}. \tag{17}$$

3 Results and discussions

Several tests of the proposed model were carried out to explore the effects of the shell correction. The potential barriers governing the α decay of ^{212}Po and ^{294}Og are shown in Fig. 1. For α emissions, the potential barrier is often treated as a finite square well before separation and a hyperbola form of the Coulomb repulsion between fragments occur. An arbitrary adjustment of the parameters allows a rough reproduction of the experimental data. However, for the MM method, as demonstrated in Section 2, barriers are determined in a quasi-molecular shape path, adjusted according to the experimental Q_α value, and most importantly, finally corrected based on the shell energy of the parent and the heavier fragment.

In Fig. 1, the red solid lines refer to Eq. (14) and (15) for the shape-dependent evolution of the shell correction energy. Their major characteristics, such as the barrier height and outer turning point, remain the same, as indicated by the blue dashed lines, which neglect the

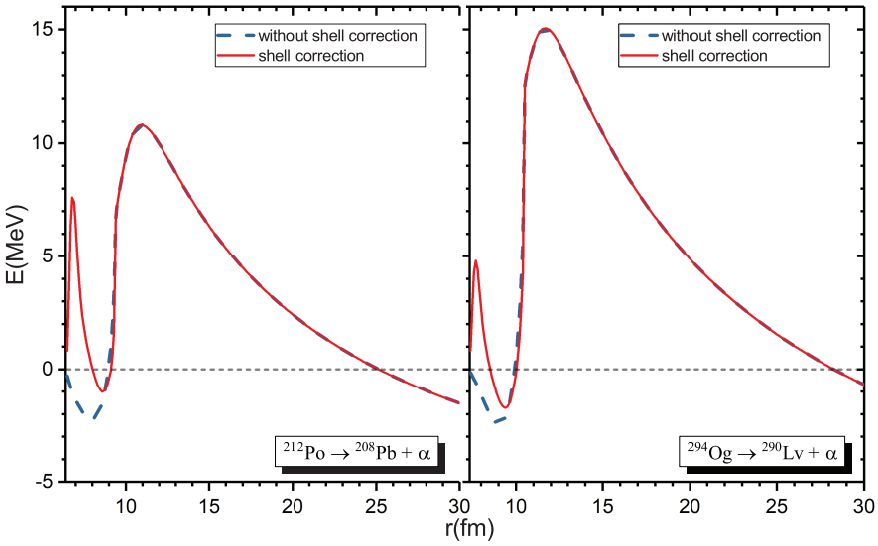

Fig. 1. (color online) The α decay barriers of ^{212}Po and ^{294}Og. The horizontal dashed line represents the energy of the spherical parent nucleus.

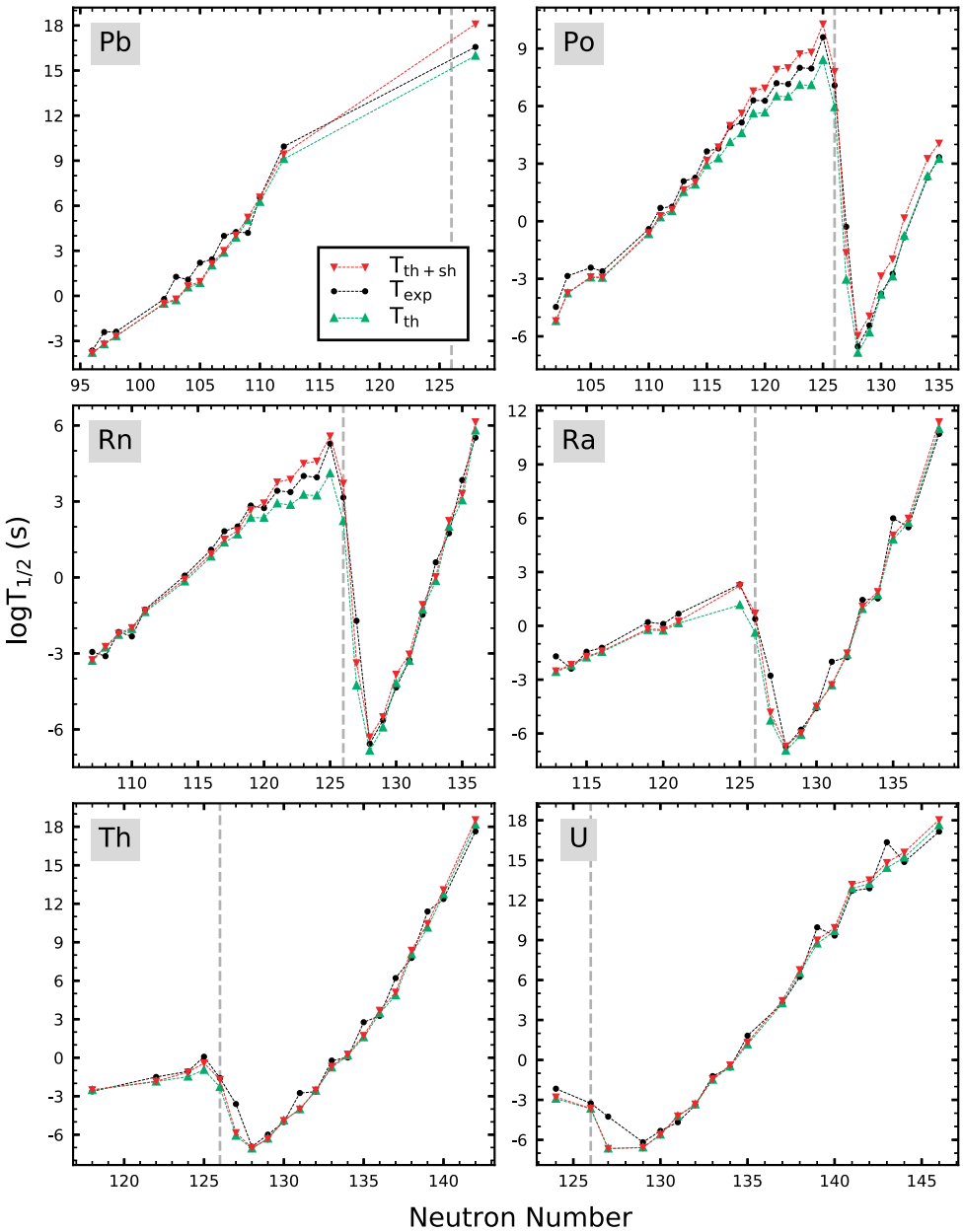

Fig. 2. (color online) Semi-log plots showing the changing trends in α decay half-lives with different partial isotopes of Pb, Po, Ra, Rn, Th, and U. Around the vertical gray dashed line (N =126), the difference between theoretical outcomes with and without a shell correction evolution, namely, the red downward triangles and green upward triangles, is noticeable. The black dots indicate the corresponding experimental values.

shell correction. However, based on the peak appearing on the left side of the plot and the increasing shallowness of the pocket, the half-lives pronouncedly change. To be more specific, the theoretical half-lives of ^{212}Po are 137.76 ns, as given by the blue dashed line when ignoring the shell correction, and 1.11 μs, as given by the red solid line with a shell correction, whereas the experimental outcome is 299 ns; in addition, for ^{294}Og, the three results are 60.01 μs, 199.63 μs, and 690 μs, respectively. The decay process is clearly hindered by the shell effects.

Additional results are listed in Table 2. For clarity and simplicity, only the favored decay channels are considered in the present paper. Comparing the data from the GLDM, there is generally a significant change in the half-lives after adding the shell correction to the barrier. Most isotopes located around neutron number 126, shown in Fig. 2, become much more stable theoretically,

which means that the shell effects hamper a significant deformation from a spherical nucleus, and therefore become a hindrance to the α emission. The RMS errors

$$\sqrt{\Sigma_{i=1}^{n}(\log T_{\rm theo}^{i}-\log T_{\rm exp}^{i})^2/n} \quad (18)$$

of both methods are listed in Table 1, which shows that our method is statistically preferable for those nuclei, with the exception of the isotopes of Pb. Incidentally, as a consequence of ignoring the pairing effects among the nucleons, the half-lives of nuclei with an odd N, for example, most of the odd isotopes of Th in Fig. 2, are underestimated.

In addition, the α decay half-lives of some superheavy nuclides are listed in Table 3. Similar to Table 2, most nuclides in Table 3 have a much longer theoretical half-life in comparison with the GLDM. However, some of the experimental data show an even longer half-life, a reasonable cause of which is a neglect of the centrifugal potential [7], leading to a lower tunneling probability and longer half-life [24]. In addition, the impact of the shell correction discussed above shows how the calculated half-lives rely on the shell correction energy of a spherical nucleus, the evaluation methods of which have still not been properly established. In addition, the reliability of current experimental data also requires further examination.

Considering the tests above, predictions for the partial α decay half-lives of the still unknown superheavy nuclei seem reliable, and are listed in Table 4. Again, similar with the results in Table 3, the half-lives are prolonged. The assumed α decay energies are calculated from the mass formula in Eq. (8) of [27]. These theoretical results may be useful for a future experimental assignment and identification.

Table 1. RMS of six isotope chain given by Eq. (18) according to the results of $\log T_{\rm th}$ and $\log T_{\rm th+sh}$ shown in Table 2. Only the favored α decay channels are involved.

Z	$\rm RMS_{th}$	$\rm RMS_{th+sh}$
Pb^{82}	0.7931	0.8243
Po^{84}	0.7933	0.6724
Rn^{86}	0.6956	0.4946
Ra^{88}	0.8221	0.6747
Th^{90}	0.8765	0.7882
U^{92}	0.8364	0.8254

Table 2. The α decay half-lives for partial isotopes of Pb, Po, Ra, Rn, Th, and U. The last column $T_{1/2}^{\rm th+sh}$ shows our results. The values in the second to last column, $T_{1/2}^{\rm th}$, were calculated using the GLDM. All theoretical results were obtained by utilizing the experimental data on Q_α from the NUBASE2012 evaluation [23]. The available $T_{1/2}^{\rm exp}$ is also extracted from [23]. Only favored α decay channels are involved.

nuclei	Q/MeV	$E_{\rm p}^{\rm sh}$/MeV	$E_{\rm d}^{\rm sh}$/MeV	$T_{1/2}^{\rm exp}$	$T_{1/2}^{\rm th}$	$T_{1/2}^{\rm th+sh}$
$^{178}_{96}$Pb	7.79	0.88	2.19	230.00 μs	161.04 μs	161.34 μs
$^{179}_{97}$Pb	7.60	1.02	2.62	3.90 ms	603.30 μs	609.73 μs
$^{180}_{98}$Pb	7.42	1.05	2.92	4.10 ms	2.08 ms	2.11 ms
$^{184}_{102}$Pb	6.77	1.52	2.93	612.50 ms	295.02 ms	321.27 ms
$^{185}_{103}$Pb	6.70	1.75	3.39	18.53 s	506.42 ms	607.51 ms
$^{186}_{104}$Pb	6.47	1.86	3.73	12.05 s	3.61 s	4.54 s
$^{187}_{105}$Pb	6.39	1.86	3.95	2.67 m	7.13 s	8.99 s
$^{188}_{106}$Pb	6.11	1.74	4.06	4.50 m	1.78 m	2.34 m
$^{189}_{107}$Pb	5.92	1.51	4.07	2.71 h	12.37 m	17.23 m
$^{190}_{108}$Pb	5.70	1.16	3.94	4.93 h	2.10 h	3.06 h
$^{191}_{109}$Pb	5.46	0.70	3.70	4.35 h	1.25 d	1.97 d
$^{192}_{110}$Pb	5.22	0.11	3.34	41.20 d	20.64 d	43.10 d
$^{194}_{112}$Pb	4.74	1.38	2.28	278.69 y	40.26 y	88.84 y
$^{210}_{128}$Pb	3.79	-10.24	-10.76	1.17 Gy	302.65 My	39.42 Gy
$^{186}_{102}$Po	8.50	4.57	0.73	34.00 μs	6.21 μs	6.43 μs
$^{187}_{103}$Po	7.98	4.84	1.19	1.40 ms	173.58 μs	183.72 μs
$^{189}_{105}$Po	7.69	5.03	1.75	3.80 ms	1.16 ms	1.25 ms
$^{190}_{106}$Po	7.69	4.91	1.86	2.46 ms	1.12 ms	1.20 ms
$^{194}_{110}$Po	6.99	3.28	1.16	392.00 ms	210.54 ms	249.54 ms
$^{195}_{111}$Po	6.75	2.60	0.70	4.94 s	1.59 s	1.95 s
$^{196}_{112}$Po	6.66	1.79	0.11	5.67 s	3.31 s	4.13 s
$^{197}_{113}$Po	6.41	0.88	-0.57	2.03 m	33.19 s	43.63 s
$^{198}_{114}$Po	6.31	-0.16	1.38	3.09 m	1.34 m	1.84 m
$^{199}_{115}$Po	6.08	-0.70	2.31	1.22 h	13.80 m	24.99 m
$^{200}_{116}$Po	5.98	-1.34	-3.34	1.73 h	31.54 m	2.06 h

Continued on the next page

Table 2. – continued from the previous page

nuclei	Q/MeV	$E_{\rm p}^{\rm sh}$/MeV	$E_{\rm d}^{\rm sh}$/MeV	$T_{1/2}^{\rm exp}$	$T_{1/2}^{\rm th}$	$T_{1/2}^{\rm th+sh}$
$^{201}_{117}$Po	5.80	-2.07	-3.91	23.01 h	3.65 h	1.12 d
$^{202}_{118}$Po	5.70	-2.89	-4.56	1.61 d	10.76 h	4.92 d
$^{203}_{119}$Po	5.50	-3.48	-5.31	23.17 d	4.76 d	71.16 d
$^{204}_{120}$Po	5.49	-4.18	-6.15	21.88 d	5.30 d	100.25 d
$^{205}_{121}$Po	5.33	-4.97	-6.74	181.25 d	37.49 d	2.60 y
$^{206}_{122}$Po	5.33	-5.86	-7.43	161.47 d	35.76 d	3.14 y
$^{207}_{123}$Po	5.22	-6.83	-8.21	3.15 y	145.87 d	16.75 y
$^{208}_{124}$Po	5.22	-7.91	-9.09	2.90 y	142.73 d	20.25 y
$^{209}_{125}$Po	4.98	-8.63	-10.06	124.00 y	7.97 y	600.55 y
$^{210}_{126}$Po	5.41	-9.42	-11.13	138.38 d	10.12 d	2.01 y
$^{211}_{127}$Po	7.59	-8.17	-11.85	516.00 ms	892.07 μs	22.87 ms
$^{212}_{128}$Po	8.95	-7.01	-12.67	294.70 ns	137.76 ns	1.11 μs
$^{213}_{129}$Po	8.54	-5.93	-11.41	3.71 μs	1.59 μs	11.45 μs
$^{214}_{130}$Po	7.83	-4.93	-10.24	163.72 μs	149.16 μs	1.39 ms
$^{215}_{131}$Po	7.53	-4.01	-9.14	1.78 ms	1.31 ms	10.78 ms
$^{216}_{132}$Po	6.91	-3.18	-8.14	145.00 ms	172.34 ms	1.47s
$^{218}_{134}$Po	6.11	-1.78	-6.38	3.10 m	3.75 m	30.51 m
$^{219}_{135}$Po	5.92	-1.20	0.00	36.52 m	29.40 m	3.22 h
$^{193}_{107}$Rn	8.04	7.20	5.03	1.15 ms	507.53 μs	561.60 μs
$^{194}_{108}$Rn	7.86	6.85	4.91	780.00 μs	1.70 ms	1.87 ms
$^{195}_{109}$Rn	7.69	6.38	4.68	7.00 ms	5.40 ms	6.13 ms
$^{196}_{110}$Rn	7.62	5.81	4.33	4.70 ms	9.16 ms	10.31 ms
$^{197}_{111}$Rn	7.41	5.12	3.86	54.00 ms	42.87 ms	48.65 ms
$^{200}_{114}$Rn	7.04	2.38	1.79	1.18 s	693.57 ms	857.91 ms
$^{202}_{116}$Rn	6.77	1.23	-0.16	12.44 s	6.66 s	8.67 s
$^{203}_{117}$Rn	6.63	0.52	-0.70	1.11 m	23.87 s	32.36 s
$^{204}_{118}$Rn	6.55	-0.28	-1.34	1.72 m	49.93 s	1.18 m
$^{205}_{119}$Rn	6.39	-0.89	-2.07	11.50 m	3.80 m	7.89 m
$^{206}_{120}$Rn	6.38	-1.60	-2.89	9.15 m	3.78 m	14.46 m
$^{207}_{121}$Rn	6.25	-2.40	-3.48	44.05 m	13.90 m	1.61 h
$^{208}_{122}$Rn	6.26	-3.30	-4.18	39.27 m	12.20 m	2.07 h
$^{209}_{123}$Rn	6.16	-4.28	-4.97	2.82 h	30.45 m	8.75 h
$^{210}_{124}$Rn	6.16	-5.36	-5.86	2.50 h	28.47 m	10.75 h
$^{211}_{125}$Rn	5.97	-6.07	-6.83	2.22 d	3.59 h	4.43 d
$^{212}_{126}$Rn	6.38	-6.84	-7.91	23.90m	2.80 m	1.45 h
$^{213}_{127}$Rn	8.25	-5.60	-8.63	19.50 ms	54.41 μs	422.40 μs
$^{214}_{128}$Rn	9.21	-4.45	-9.42	270.00 ns	144.30 ns	505.11 ns
$^{215}_{129}$Rn	8.84	-3.38	-8.17	2.30 μs	1.19 μs	3.15 μs
$^{216}_{130}$Rn	8.20	-2.39	-7.01	45.00 μs	66.71 μs	150.08 μs
$^{217}_{131}$Rn	7.89	-1.49	-5.93	540.00 μs	503.12 μs	936.11 μs
$^{218}_{132}$Rn	7.26	-0.67	-4.93	33.75 ms	53.58 ms	84.80 ms
$^{219}_{133}$Rn	6.95	0.07	-4.01	3.96 s	719.61 ms	1.08 s
$^{220}_{134}$Rn	6.40	0.73	-3.18	55.60 s	1.65 m	2.93 m
$^{221}_{135}$Rn	6.16	1.29	-2.44	1.95 h	18.35 m	34.32 m
$^{222}_{136}$Rn	5.59	1.78	-1.78	3.82 d	7.31 d	16.05 d
$^{201}_{113}$Ra	8.00	5.33	5.12	20.00 ms	2.67 ms	3.03 ms
$^{202}_{114}$Ra	7.88	4.31	4.32	4.10 ms	6.14 ms	6.91 ms
$^{203}_{115}$Ra	7.74	3.79	3.41	36.00 ms	17.21 ms	19.35 ms
$^{204}_{116}$Ra	7.64	3.18	2.38	60.00 ms	34.86 ms	38.94 ms
$^{207}_{119}$Ra	7.27	1.08	0.52	1.60 s	587.11 ms	668.82 ms
$^{208}_{120}$Ra	7.27	0.36	-0.28	1.28 s	539.78 ms	611.66 ms
$^{209}_{121}$Ra	7.14	-0.44	-0.89	4.71 s	1.40 s	1.80 s
$^{213}_{125}$Ra	6.86	-4.12	-4.28	3.41 m	14.45 s	2.84 m
$^{214}_{126}$Ra	7.27	-4.89	-5.36	2.44 s	407.91 ms	5.05 s

Continued on the next page

Table 2. – continued from the previous page

$^{215}_{127}$Ra	8.86	-3.67	-6.07	1.67 ms	5.17 μs	15.23 μs
$^{216}_{128}$Ra	9.53	-2.53	-6.84	182.00 ns	109.40 ns	199.56 ns
$^{217}_{129}$Ra	9.16	-1.46	-5.60	1.63 μs	817.57 ns	1.09 μs
$^{218}_{130}$Ra	8.55	-0.48	-4.45	25.20 μs	33.28 μs	32.71 μs
$^{219}_{131}$Ra	8.14	0.41	-3.38	10.00 ms	485.14 μs	519.69 μs
$^{220}_{132}$Ra	7.59	1.22	-2.39	17.90 ms	24.95 ms	30.33 ms
$^{221}_{133}$Ra	6.88	1.95	-1.49	28.00 s	8.67 s	12.47 s
$^{222}_{134}$Ra	6.68	2.59	-0.67	33.60 s	53.68 s	1.33 m
$^{223}_{135}$Ra	5.98	3.16	0.07	11.44 d	18.18 h	1.33 d
$^{224}_{136}$Ra	5.79	3.63	0.73	3.63 d	6.47 d	11.55 d
$^{226}_{138}$Ra	4.87	5.58	1.78	1.60 ky	3.02 ky	7.43 ky
$^{208}_{118}$Th	8.20	3.12	3.18	2.40 ms	3.00 ms	3.16 ms
$^{212}_{122}$Th	7.96	0.02	0.36	31.70 ms	13.82 ms	14.58 ms
$^{214}_{124}$Th	7.83	-2.09	-1.35	87.00 ms	33.78 ms	75.80 ms
$^{215}_{125}$Th	7.67	-2.76	-2.35	1.20 s	112.30 ms	382.27 ms
$^{216}_{126}$Th	8.07	-3.53	-3.44	26.00 ms	5.20 ms	19.91 ms
$^{217}_{127}$Th	9.44	-2.31	-4.12	247.00 μs	826.59 ns	1.44 μs
$^{218}_{128}$Th	9.85	-1.18	-4.89	117.00 ns	83.44 ns	95.00 ns
$^{219}_{129}$Th	9.51	-0.14	-3.67	1.02 μs	495.39 ns	476.61 ns
$^{220}_{130}$Th	8.95	0.83	-2.53	9.70 μs	12.65 μs	12.65 μs
$^{221}_{131}$Th	8.63	1.71	-1.46	1.78 ms	95.54 μs	98.70 μs
$^{222}_{132}$Th	8.13	2.51	-0.48	2.24 ms	2.69 ms	2.98 ms
$^{223}_{133}$Th	7.57	3.23	0.41	600.00 ms	172.98 ms	210.01 ms
$^{224}_{134}$Th	7.30	3.86	1.22	1.04 s	1.49 s	1.88 s
$^{225}_{135}$Th	6.92	4.42	1.95	9.72 m	39.29 s	53.33 s
$^{226}_{136}$Th	6.45	4.89	2.59	30.70 m	49.67 m	1.37 h
$^{227}_{137}$Th	6.15	5.85	3.16	18.70 d	20.23 h	1.47 d
$^{228}_{138}$Th	5.52	6.72	3.63	1.91 y	3.73 y	7.48 y
$^{229}_{139}$Th	5.17	7.47	4.66	7.92 ky	433.87 y	907.07 y
$^{230}_{140}$Th	4.77	8.13	5.58	75.40 ky	177.25 ky	388.10 ky
$^{232}_{142}$Th	4.08	9.13	7.12	14.00 Gy	46.44 Gy	111.82 Gy
$^{216}_{124}$U	8.53	-1.28	0.02	6.90 ms	1.21 ms	1.63 ms
$^{218}_{126}$U	8.78	2.71	-2.09	550.00 μs	215.77 μs	227.37 μs
$^{219}_{127}$U	9.94	1.51	-2.76	55.00 μs	220.75 ns	222.06 ns
$^{221}_{129}$U	9.89	0.63	-2.31	660.00 ns	265.13 ns	263.21 ns
$^{222}_{130}$U	9.48	1.58	-1.18	4.70 μs	2.45 μs	2.52 μs
$^{223}_{131}$U	8.95	2.45	-0.14	21.00 μs	59.43 μs	61.11 μs
$^{224}_{132}$U	8.63	3.25	0.83	396.00 μs	452.48 μs	482.45 μs
$^{225}_{133}$U	8.02	3.96	1.71	61.00 ms	32.58 ms	36.90 ms
$^{226}_{134}$U	7.70	4.58	2.51	269.00 ms	318.59 ms	409.24 ms
$^{227}_{135}$U	7.23	5.12	3.23	1.10 m	14.66 s	20.59 s
$^{229}_{137}$U	6.48	6.49	4.42	4.82 h	4.89 h	7.91 h
$^{230}_{138}$U	5.99	7.29	4.89	20.23 d	39.57 d	68.83 d
$^{231}_{139}$U	5.58	7.99	5.85	287.48 y	17.50 y	31.92 y
$^{232}_{140}$U	5.41	8.58	6.72	68.90 y	149.11 y	274.50 y
$^{233}_{141}$U	4.91	9.08	7.47	159.20 ky	239.94 ky	480.22 ky
$^{234}_{142}$U	4.86	9.48	8.13	245.50 ky	533.22 ky	1.04 My
$^{235}_{143}$U	4.68	9.77	8.68	704.00 My	8.42 My	20.81 My
$^{236}_{144}$U	4.57	9.97	9.13	23.42 My	50.86 My	125.16 My
$^{238}_{146}$U	4.27	10.06	9.73	4.47 Gy	13.60 Gy	34.60 Gy

Table 3. Comparison between the experimental and calculated half-life values of some superheavy elements. These experimental data in the decay chain of ^{294}Ts (shown with the asterisk) are from[25], and the other data are from[23, 26]. Only the favored α decay channels are involved.

Ele.	nuclei	Q/MeV	$E_{\rm p}^{shell}$/MeV	$E_{\rm d}^{shell}$/MeV	$T_{1/2}^{exp}$	$T_{1/2}^{th}$	$T_{1/2}^{th+sh}$
Db*	$^{270}_{165}$105	8.02	4.28	6.13	1.32 h	10.92 m	15.73 m
Bh*	$^{274}_{167}$107	8.82	2.92	4.28	42 s	5.02 s	6.67 s
Hs	$^{278}_{169}$109	9.51	1.13	2.92	290 ms	161.22 ms	175.37 ms
Rg*	$^{282}_{171}$111	9.13	-0.80	1.13	2.1 min	10.17 s	19.76 s
Nh	$^{285}_{172}$113	9.61	-2.79	-0.80	5.6 s	1.48 s	5.86 s
Nh*	$^{286}_{173}$113	9.74	-2.85	-0.80	7.9 s	585.85 ms	2.23 s
Fl	$^{286}_{172}$114	10.33	-3.85	-1.75	140 ms	26.44 ms	106.81 ms
Mc	$^{289}_{174}$115	10.34	-3.86	-2.79	0.38 s	46.53 ms	190.92 ms
Mc*	$^{290}_{175}$115	9.91	-4.07	-2.85	0.75 s	759.68 ms	4.45 s
Lv	$^{290}_{174}$116	11.00	-3.77	-3.85	8 ms	1.63 ms	5.38 ms
Ts	$^{293}_{176}$117	10.74	-4.22	-3.86	27 ms	14.19 ms	58.36 ms
Ts*	$^{294}_{177}$117	10.96	-4.57	-4.07	51 ms	3.85 ms	16.57 ms
Og	$^{294}_{176}$118	11.82	-4.29	-3.77	0.69 ms	60.01 μs	199.63 μs

Table 4. Prediction of α decay half-lives using the macroscopic-microscopic method. The atomic number ranges from 290 to 310 for both unknown elements 119 and 120. The α energies are taken from [27]. Only the favored α decay channels are involved.

nuclei	Q/MeV	$E_{\rm p}^{shell}$/MeV	$E_{\rm d}^{shell}$/MeV	$T_{1/2}^{th}$	$T_{1/2}^{th+sh}$
$^{290}_{171}$119	13.17	-3.66	-3.36	184.73 ns	455.27 ns
$^{291}_{172}$119	13.05	-3.69	-3.53	309.97 ns	781.11 ns
$^{292}_{173}$119	12.92	-3.77	-3.49	535.35 ns	1.38 μs
$^{293}_{174}$119	12.80	-3.93	-3.53	924.81 ns	2.46 μs
$^{294}_{175}$119	12.67	-4.14	-3.60	1.64 μs	4.64 μs
$^{295}_{176}$119	12.55	-4.43	-3.74	2.76 μs	8.57 μs
$^{296}_{177}$119	12.42	-4.77	-3.95	4.98 μs	17.46 μs
$^{297}_{178}$119	12.29	-5.19	-4.22	8.98 μs	36.15 μs
$^{298}_{179}$119	12.16	-5.10	-4.57	16.78 μs	68.65 μs
$^{299}_{180}$119	12.03	-5.07	-4.97	31.54 μs	130.83 μs
$^{300}_{181}$119	11.90	-4.92	-4.89	62.17 μs	250.28 μs
$^{301}_{182}$119	11.77	-4.85	-4.86	121.06 μs	507.44 μs
$^{302}_{183}$119	11.63	-4.84	-4.74	243.51 μs	1.06 ms
$^{303}_{184}$119	11.50	-4.89	-4.68	486.67 μs	2.16 ms
$^{304}_{185}$119	11.37	-3.73	-4.69	978.71 μs	3.17 ms
$^{305}_{186}$119	11.23	-2.64	-4.76	2.06 ms	4.88 ms
$^{306}_{187}$119	11.10	-1.60	-3.59	4.48 ms	7.84 ms
$^{307}_{188}$119	10.97	-0.63	-2.50	9.68 ms	11.77 ms
$^{308}_{189}$119	10.83	0.28	-1.46	21.88 ms	21.71 ms
$^{309}_{190}$119	10.69	1.12	-0.48	49.50 ms	51.23 ms
$^{310}_{191}$119	10.56	1.90	0.42	116.29 ms	124.26 ms
$^{290}_{170}$120	13.70	-3.89	-3.29	35.73 ns	89.23 ns
$^{291}_{171}$120	13.58	-3.85	-3.41	58.37 ns	146.48 ns
$^{292}_{172}$120	13.46	-3.87	-3.58	93.76 ns	239.25 ns
$^{293}_{173}$120	13.33	-3.96	-3.54	157.40 ns	395.25 ns
$^{294}_{174}$120	13.21	-4.12	-3.57	259.81 ns	710.68 ns
$^{295}_{175}$120	13.08	-4.34	-3.65	423.18 ns	1.21 μs
$^{296}_{176}$120	12.96	-4.63	-3.80	706.24 ns	2.25 μs
$^{297}_{177}$120	12.83	-4.98	-4.01	1.23 μs	4.39 μs
$^{298}_{178}$120	12.71	-5.41	-4.29	2.17 μs	8.68 μs
$^{299}_{179}$120	12.57	-5.32	-4.63	3.97 μs	15.95 μs
$^{300}_{180}$120	12.45	-5.27	-5.04	7.11 μs	28.75 μs

Continued on the next page

Table 4. – continued from the previous page

nuclei	Q/MeV	$E_{\rm p}^{shell}$/MeV	$E_{\rm d}^{shell}$/MeV	$T_{1/2}^{th}$	$T_{1/2}^{th+sh}$
$^{301}_{181}120$	12.32	-5.13	-4.96	13.35 μs	54.21 μs
$^{302}_{182}120$	12.19	-5.05	-4.93	24.60 μs	101.19 μs
$^{303}_{183}120$	12.06	-5.03	-4.79	47.12 μs	195.22 μs
$^{304}_{184}120$	11.93	-5.08	-4.72	85.78 μs	355.65 μs
$^{305}_{185}120$	11.79	-3.92	-4.72	173.10 μs	548.83 μs
$^{306}_{186}120$	11.67	-2.83	-4.78	342.52 μs	803.38 μs
$^{307}_{187}120$	11.53	-1.81	-3.62	708.17 μs	1.26 ms
$^{308}_{188}120$	11.40	-0.85	-2.53	1.44 ms	1.87 ms
$^{309}_{189}120$	11.26	0.05	-1.49	3.08 ms	2.99 ms
$^{310}_{190}120$	11.13	0.88	-0.51	6.66 ms	6.75 ms

4 Summary

We considered the GLDM and a shell correction as the macroscopic and microscopic terms for the total energy, respectively. For the sake of completeness, the form of the shell correction is related not only to the deformation of the mother nucleus, but also to its ensuing deformation process when breaking into two fragments.

Within the vicinity of the point where two spherical nuclei make contact, the alterations of the barriers as compared with the GLDM are considerable, namely, a peak appears before the saddle point, and the minimum between them is much closer to the ground state energy. Correspondingly, larger half-lives are obtained for heavy and superheavy α emitters, which may indicate a higher probability for the existence of unknown superheavy nuclei.

Temporarily, for congruity of the shell correction energy, the shell correction of the heavier fragment is assumed to change linearly with the distance between the mass centers of the two quasi-fragments. In addition, the treatment of small deformations in two-body potentials remains absent. After giving full consideration to the shell correction during the entire α decay process, we expect to refine the approach in a future study.

References

1 E. Rutherford et al, Proc. R. Soc. A Math. Phys. Eng. Sci., **123**: 373 (1929)
2 C. F. v. Weizsäcker, Zeitschrift für Phys., **96**: 431 (1935)
3 N. Bohr and J. A. Wheeler, Phys. Rev., **56**: 426 (1939)
4 L. To et al, J. Phys. G Nucl. Phys., **8**: L159 (1982)
5 G. Royer and B. Remaud, J. Phys. G Nucl. Phys., **9**: 1103 (1983)
6 X. Bao, H. Zhang, G. Royer, and J. Li, Nucl. Phys. A, **906**: 1 (2013)
7 G. Royer and B. Remaud, Nucl. Physics, Sect. A, **444**: 477 (1985)
8 X. J. Bao, H. F. Zhang, B. S. Hu, G. Royer, and J. Q. Li, J. Phys. G Nucl. Part. Phys., **39**: 095103 (2012)
9 J. M. Dong, H. F. Zhang, and G. Royer, Phys. Rev. C., **79**: 54330 (2009)
10 G. Royer, J. Phys. G Nucl. Part. Phys., **26**: 1149 (2000)
11 G. Royer, A. Escudie, and B. Sublard, **024607**: 1 (2014)
12 G. Royer, N. Mokus, and J. Jahan, Phys. Rev. C, **95**: 054610 (2017)
13 P. Möller, A. J. Sierk, T. Ichikawa, and H. Sagawa, At. Data Nucl. Data Tables, **109-110**: 1 (2016), 9308022
14 W. D. Myers and W. J. Swiatecki, Nucl. Phys., **81**: 1 (1966)
15 V. M. Strutinsky, Nucl. Phys. A, **95**: 420 (1967)
16 G. Royer and B. Remaud, J. Phys. G Nucl. Phys., **10**: 1057 (1984)
17 Y. Qian and Z. Ren, Nucl. Phys. A, **852**: 82 (2011)
18 Y. Qian and Z. Ren, J. Phys. G Nucl. Part. Phys., **45**: 035103 (2018)
19 H. Feldmeier, 12^{th} Summer School on Nuclear Physics, Mikolajki, 1979
20 W. D. Myers, Droplet Model of Atomic Nuclei, (New-York: Plennum, 1997)
21 S. Cwiok, J. Dudek, W. Nazarewicz, J. Skalski, and T. Werner, Comput. Phys. Commun., **46**: 379 (1987)
22 W. D. Myers and W. J. Swiatecki, Nucl. Phys. A, **601**: 141 (1996)
23 G. Audi *et al.*: Chinese Phys. C, **36**: 1157 (2012)
24 H. Zhang, W. Zuo, J. Li, and G. Royer, Phys. Rev. C., **74**: 17304 (2006)
25 J. Khuyagbaatar et al, Phys. Rev. Lett., **112**: 1 (2014)
26 Y. T. Oganessian et al, Phys. Rev. Lett., **109**: 162501 (2012)
27 G. Royer, M. Guilbaud, and A. Onillon, Nucl. Phys. A, **847**: 24 (2010)